



# Tuning the magnetocrystalline anisotropy of rare-earth free $L1_0$ -ordered $Mn_{1-x}TM_xAl$ magnetic alloy (TM = Fe, Co, or Ni) with transition elements

Minyeong Choi<sup>a</sup>, Yang-Ki Hong<sup>a,\*</sup>, Hoyun Won<sup>a</sup>, Chang-Dong Yeo<sup>b,\*</sup>, Nayem M.R. Shah<sup>b</sup>,  
Byoung-Chul Choi<sup>c</sup>, Woncheol Lee<sup>a,d</sup>, Haein Choi-Yim<sup>e</sup>, Wooyoung Lee<sup>f</sup>, Jan-Ulrich Thiele<sup>g</sup>

<sup>a</sup> Department of Electrical and Computer Engineering, The University of Alabama, Tuscaloosa, AL 35487, USA

<sup>b</sup> Department of Mechanical Engineering, Texas Tech University, Lubbock, TX 79409, USA

<sup>c</sup> Department of Physics and Astronomy, University of Victoria, Victoria, BC V8W 2Y2, Canada

<sup>d</sup> Samsung Electronics Co., Ltd., Suwon, Republic of Korea

<sup>e</sup> Department of Applied Physics, Sookmyung Women's University, Seoul 04310, Republic of Korea

<sup>f</sup> Department of Materials Science and Engineering, Yonsei University, Seoul 03722, Republic of Korea

<sup>g</sup> Seagate Technology LLC, Fremont, CA 94538, USA

## ARTICLE INFO

### Keywords:

First-principles calculations  
Hard magnetic material  
Magnetic properties  
Rare-earth free  $L1_0$ -ordered magnetic alloy

## ABSTRACT

Tuning of the magnetocrystalline anisotropy of MnAl was studied by substituting Mn of MnAl with transition elements (Fe, Co, or Ni). The Brillouin function and semi-empirical Callen and Callen relation predicted the thermal behaviors of saturation magnetization and magnetocrystalline anisotropy energy. First-principles calculations based on density functional theory (DFT) were performed to calculate the electronic structures of  $Mn_{0.5}TM_{0.5}Al$ , where TM = Mn, Fe, Co, and Ni. The estimated total magnetic moment of  $Mn_{0.5}TM_{0.5}Al$  decreases as the number of valence electrons ( $n$ ) of TM (e.g., 7 for Mn ( $3d^5 4s^2$ ), 8 for Fe ( $3d^6 4s^2$ ), 9 for Co ( $3d^7 4s^2$ ), and 10 for Ni ( $3d^8 4s^2$ )) increases. Ni-substituted MnAl becomes ferrimagnetic, while other TM-substituted MnAl retain a ferromagnetic state. Curie temperature rapidly decreases with increasing the valence electrons from 685 K for MnAl to 20 K for Ni-substituted MnAl. Thermomagnetic behaviors of  $Mn_{0.5}TM_{0.5}Al$  (TM = Mn, Fe, Co, or Ni) are reported. Our magnetocrystalline anisotropy energy (MAE) calculations demonstrate that the magnetocrystalline anisotropy changes to the in-plane from the out-of-plane (uniaxial) direction for Co- and Ni-substituted MnAl. The  $K$  reaches a maximum of 2.98 MJ/m<sup>3</sup> at  $n = 8$ , i.e., Fe substitution.

## 1. Introduction

Consumption of rare-earth (RE) elements, in particular, Nd and Dy, will outstrip the global supply within a decade due to skyrocketing demand for electric vehicles (EVs), wind turbine generators, and other energy applications requiring permanent magnets (PMs) [1]. PMs play a crucial role in energy technologies. Therefore, RE-free permanent magnets are emerging for scientific and technological interests.

A permanent magnet (PM) needs a high magnetocrystalline anisotropy; therefore, a high maximum energy product  $(BH)_{max}$ . Accordingly, manganese (Mn)-based alloys have been proposed as promising candidates for rare-earth-free permanent magnets. The RE-free  $L1_0$ -ordered MnAl alloys received much attention [2,3]. Mn has the highest magnetic moment among transition metals (TMs) [4] and is inexpensive. However, the Mn element is antiferromagnetic due to direct exchange

coupling between Mn atoms when the distance between them is close to 2.83 Å [5,6] but becomes ferromagnetic when it alloys with Al. The exchange integral changes its sign at a considerable distance between the Mn atoms. The  $L1_0$ -ordered MnAl shows potential in achieving higher saturation magnetization ( $M_S$ ) and  $(BH)_{max}$  than those of Nd-Fe-B above 473 K due to its high  $T_C$  of 650 K but lower magnetization below 473 K [7] and unstable ferromagnetic  $\tau$  phase. Improvement in  $(BH)_{max}$  requires minimization of Mn-Mn antiferromagnetic interactions in Mn-Al, narrowing of anisotropy distribution, breakdown in intergranular exchange, and thermal stability of  $\tau$ -phase. The improvement seems difficult unless the third element is added to MnAl. Therefore, we have inserted a carbon atom into the  $(\frac{1}{2}, \frac{1}{2}, \frac{1}{2})$  site of the  $L1_0$ -ordered MnAl unit cell to study  $\tau$ -phase phase stability using first-principles calculations based on density functional theory. It was found that a carbon content of 2.33 at% gives the most stable  $\tau$ -phase  $L1_0$

\* Corresponding authors.

E-mail addresses: [ykhong@eng.ua.edu](mailto:ykhong@eng.ua.edu) (Y.-K. Hong), [Changdong.yeo@ttu.edu](mailto:Changdong.yeo@ttu.edu) (C.-D. Yeo).

<https://doi.org/10.1016/j.jmmm.2023.171513>

Received 6 August 2022; Received in revised form 21 October 2023; Accepted 7 November 2023

Available online 11 November 2023

0304-8853/© 2023 Elsevier B.V. All rights reserved.

(Mn<sub>0.5</sub>Al<sub>0.5</sub>)<sub>100-x</sub>C<sub>x</sub> that has the lowest formation energy and highest saturation magnetization among the studied carbon contents ( $x = 0-3.03$  at%) [8]. It is noted that a change in magnetocrystalline anisotropy ( $K$ ) with carbon addition was not noticeable.

On the other hand, TM (transition element)-doped Mn-Al, such as Fe [9,10], Co [11], Ni [12,13], and Cu [14-16], have been studied for magnetic properties. Manchanda *et al.* performed the first-principles calculation on Fe-doped  $L1_0$ -ordered MnAl (Mn<sub>16-x</sub>Fe<sub>x</sub>Al<sub>16</sub>) [10]. The calculated total magnetic moment per supercell decreased to 34.01  $\mu_B$  at  $x = 10.6$  (Mn<sub>8</sub>Fe<sub>8</sub>Al<sub>16</sub>) from 38.06  $\mu_B$  (Mn<sub>16</sub>Al<sub>16</sub>;  $x = 0.0$ ) at 0 K, but  $K$  increased by 41.2 % from 1.77 MJ/m<sup>3</sup> for Mn<sub>16</sub>Al<sub>16</sub> to 2.5 MJ/m<sup>3</sup> for Mn<sub>8</sub>Fe<sub>8</sub>Al<sub>16</sub>. However, the theoretical  $T_C$  and temperature-dependent magnetic properties of Fe-doped Mn-Al were not reported. Xiang *et al.* found an increase in lattice constant  $a$  and a decrease in lattice constant  $c$  by doping  $L1_0$ -ordered Mn<sub>55</sub>Al<sub>45</sub> with Co [11]. The saturation magnetization ( $M_S$ ) and intrinsic coercivity ( $H_{ci}$ ) increased by 3 at% Co addition, therefore higher  $(BH)_{max}$ . This is attributed to the stabilization of the  $\tau$ -phase Mn-Al by Co-doping. Feng *et al.* studied Ni-doped MnAl-C and found that 0.6 at% Ni doping results in  $M_S$  of 0.73 T,  $H_{ci}$  of 3.2 kOe, and  $(BH)_{max}$  of 6.16 MGOe [12]. Morisako *et al.* experimentally found that the phase of Mn<sub>60-x</sub>Al<sub>40</sub>Ni<sub>x</sub> ( $x = 0 \sim 35$ ) sputtered thin film changed to  $\kappa$ -phase at 7 at% Ni from the  $\tau$ -phase ( $L1_0$ -ordered structure) at  $x = 0.0$  [13]. As Ni concentration increases, the lattice constant  $a$  increases, and lattice constant  $c$  decreases. The  $M_S$  and  $H_{ci}$  increase from 120 emu/cc and 2 kOe to 200 emu/cc and 3 kOe, respectively, at 3 at% Ni. Recently, Feng *et al.* reported that Ni addition to MnAl-C improves the squareness of the demagnetization curve by reducing the highly twinned non-recrystallized regions [17]. For Cu-substituted Mn-Al, the substitution decreased  $M_S$ , remanent magnetization ( $M_r$ ),  $H_{ci}$ , and  $(BH)_{max}$  but did not affect  $T_C$  in the range of Cu concentration (0 ~ 6 at%) [14].

All the above studies confirm that TM ferromagnetic element is crucial in modifying the magnetic properties of RE-free  $L1_0$ -ordered Mn-Al. However, TM-doping-related magnetocrystalline anisotropy energy, including anisotropy direction change with TM elements, has not been thoroughly studied. Magnetocrystalline anisotropy energy (MAE:  $H_K$  or  $K$  (anisotropy constant)) is one of two key factors ( $M_S$  and  $H_c$ ) determining the  $(BH)_{max}$  of an anisotropic permanent magnet. Magnetic anisotropy of  $L1_0$ -ordered Mn-Al can be tuned but not comprehensively studied yet. Furthermore, no report exists on the  $M_S(T)$  and  $K(T)$  for Mn<sub>0.5</sub>TM<sub>0.5</sub>Al, where TM is Fe, Co, or Ni. MAE is subject to the nature of the electronic structure near the Fermi energy, suggesting that the MAE could be controlled by tuning the band structure around the Fermi energy by doping MnAl with TM.

In this paper, we report the electronic structures of TM (Fe, Co, Ni)-doped  $L1_0$ -ordered MnAl; therefore, MAE, otherwise anisotropy constant ( $K$ ), saturation magnetization ( $M_S$ ), Curie temperature ( $T_C$ ),  $c/a$  (lattice constants) ratio effect (*i.e.*, strain) on  $K$ ,  $M_S(T)$ , and  $K(T)$ . First-principles calculations based on density functional theory (DFT) were performed, as implemented in the WIEN2k code [18]. In particular, it was found that the anisotropy of  $L1_0$ -ordered MnAl changes from the out-of-plane direction to the in-plane direction with substitutional Co or Ni doping.

## 2. CRYSTAL STRUCTURE AND CALUCLATION MTHOD

### A. Crystal Structure.

Fig. 1 shows the crystal structure of TM (Fe, Co, Ni)-doped  $L1_0$ -ordered MnAl. The Mn<sub>0.5</sub>TM<sub>0.5</sub>Al unit cell has two Mn atoms of (0, 0, 0) and (1/2, 1/2, 0) sites and two Al atoms of (1/2, 0, 1/2) and (0, 1/2, 1/2) sites [2,19]. The TM substitutes for the Mn atom in (1/2, 1/2, 0) site of MnAl. Lattice parameters are determined after having the Mn<sub>0.5</sub>TM<sub>0.5</sub>Al unit cell relaxed and summarized in Table 1. Both the  $c/a$  ratio and volume of Mn<sub>0.5</sub>TM<sub>0.5</sub>Al decrease as the TM valence electron number ( $n$ ) increases from 7 (Mn) to 10 (Ni). For the Mn<sub>0.5</sub>TM<sub>0.5</sub>Al (TM = Mn, Fe, Co, or Ni), the following  $n$  are used in electronic structure calculations: 7 for Mn ( $3d^5 4s^2$ ), 8 for Fe ( $3d^6 4s^2$ ), 9 for Co ( $3d^7 4s^2$ ), 10

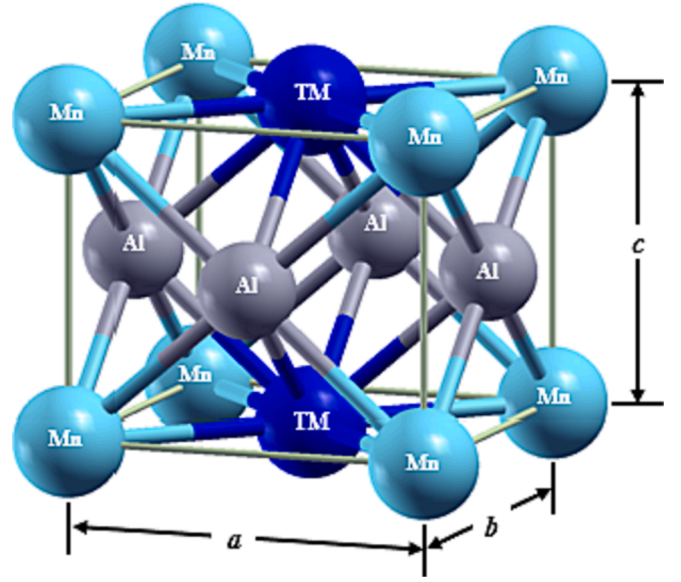


Fig. 1. Crystal structure (unit cell) of  $L1_0$ -ordered Mn<sub>0.5</sub>TM<sub>0.5</sub>Al (TM = Fe, Co, Ni) alloy.

Table 1

Lattice parameters of  $L1_0$ -ordered Mn<sub>0.5</sub>TM<sub>0.5</sub>Al.

Material	Lattice Constant (Å)		Volume (Å <sup>3</sup> )	$c/a$
	$a$	$c$		
MnAl	3.84	3.34	49.26	0.87
Mn <sub>0.5</sub> Fe <sub>0.5</sub> Al	3.85	3.21	47.65	0.84
Mn <sub>0.5</sub> Co <sub>0.5</sub> Al	4.01	2.87	46.07	0.72
Mn <sub>0.5</sub> Ni <sub>0.5</sub> Al	4.03	2.82	45.82	0.70

for Ni ( $3d^8 4s^2$ ), and 3 for Al ( $3s^2 3p^1$ ).

### 3. B. Calculation

After relaxing the unit cell volume of Mn<sub>0.5</sub>TM<sub>0.5</sub>Al (TM = Fe, Co, Ni) by minimizing the total energy to find their equilibrium lattice constants in Table 1, the Kohn-Sham equation,  $\hat{H}_{KS}\Psi(r) = \epsilon_i\Psi(r)$ , is solved with the relaxed lattice constants to calculate electronic structure. The Hamiltonian ( $\hat{H}_{KS}$ ) for the Kohn-Sham equation is expressed as

$$\hat{H}_{KS} = \sum_i \left[ -\frac{\hbar^2 \Delta_i}{2m_e} + \sum_l \frac{-e^2}{4\pi\epsilon_0} \frac{Z_l}{|r_i - R_l|} \right] + \frac{1}{2} \sum_{i,j} \frac{e^2}{4\pi\epsilon_0} \frac{1}{|r_i - r_j|} \quad (1)$$

where the first term is the kinetic energy, the second term is nuclei energy (lattice potential), and the last term is the sum of the electron exchange and correlation energies (interaction) [20].

The corresponding wave function is  $\Psi(r) = \sum C_{kn}\phi_{kn}$ , where the wave ( $\phi_{kn}$ ) consists of a partial atomic wave in an atomic sphere ( $as$ ) and a plane wave of the interstitial region ( $ir$ ) of the MnAl unit cell.

The partial atomic wave is  $\phi_{kn} = [A_{lm}^K u_l(r, \epsilon) + B_{lm}^K \dot{u}_l(r, \epsilon)] Y_{lm}(r)$ , and the plane wave is  $\phi_{kn} = e^{i(k+Kn)r}$ .  $A_{lm}^K$  and  $B_{lm}^K$  are the coefficients for matching the plane wave.  $u_l$  is the numerical solution of the radial Schrödinger equation in a given spherical potential.  $\dot{u}_l$  is the energy derivative of  $u_l$ .  $Y_{lm}$  are the spherical harmonics of angular momentum  $l$  and quantum number  $m$ .

The WIEN2k code, based on density functional theory (DFT) within the local-spin-density approximation (LSDA), with the full-potential linearized augmented plane wave (FP-LAPW) method, is used to conduct the first-principles calculations; therefore, electronic structure [18]. All calculations use  $19 \times 19 \times 27$  k-point mesh, generating 1400 k-

points in the irreducible part of the Brillouin zone.

Regarding magnetocrystalline anisotropy calculations, after adding spin-orbit coupling Hamiltonian ( $H_{so}$ ),  $H_{so} = -\frac{e\hbar}{4m^2c^2} \sigma \bullet \nabla\varphi(r) \times p = -\frac{e\hbar^2}{2m^2c^2} \frac{1}{r} \frac{d\varphi}{dr} L \bullet S$ , to the  $H_{ks}$ , where  $c$  is the speed of light,  $\varphi$  is the potential energy of the electron,  $\sigma$  is the spin,  $p$  is momentum operator,  $L$  is the orbital angular momentum, and  $S$  is the spin angular momentum [21], the Kohn-Shame equation is solved for eigenvalues  $\epsilon_i(\hat{n}_1)$  and  $\epsilon_i(\hat{n}_2)$ ; therefore, the magnetocrystalline anisotropy energy ( $\Delta E_{MAE}$ ) is calculated by Eq. (2).

where  $\hat{n}_1$  and  $\hat{n}_2$  are easy and hard spin directions, respectively. Accordingly, magnetocrystalline anisotropy energy (MAE) of Mn-TM-Al is calculated using the total energy difference between  $\langle 001 \rangle$  and  $\langle 100 \rangle$  spin configurations ( $\Delta E = E_{\langle 100 \rangle} - E_{\langle 001 \rangle}$ ), i.e., the magnetic force theorem.

To calculate the temperature (T) dependence of saturation magnetization  $M_s(T)$  and magnetocrystalline anisotropy constant  $K(T)$ , one needs Curie temperature ( $T_C$ ). The exchange integrals ( $J_{ij}$ ) are calculated for the  $T_C$  by the energy difference between the ground and excited states. The exchange integral can be expressed by  $J_{ij} = (\Delta_{ij} - \Delta_i - \Delta_j) / (4S_i S_j n_i z_{ij} \sigma_i^{(0)} \sigma_j^{(0)})$  [22], where  $S_i$  is the quantum spin of the  $i$ th Mn atom,  $\Delta_i$  is the exchange energy difference between the ground and excited states when the  $i$ th Mn atom is reversed,  $n_i$  is the number of the  $i$ th atom, and  $z_{ij}$  is the number of neighboring the  $j$ th atom to the  $i$ th atom. The exchange integrals ( $J_{ij}$ ) consider interactions over all neighboring spins, then  $J_0 = \sum_j J_{0j}$  [23]. The  $T_C$  is then calculated with  $J_0$  using the following mean-field approximation (MFA) [24]:

$$T_C = \frac{2}{3k_B} J_0 \gamma \quad (3)$$

where  $J_0$  is the molecular field parameter calculated by the summation of the exchange integrals  $J_{0j}$ , and  $k_B$  is the Boltzmann constant ( $1.38 \times 10^{-23}$  J/K). The factor  $\gamma$  equals  $S(S+1)/S^2$ , where  $S$  is the spin angular momentum.

Now,  $M_s(T)$  is expressed by Eq. (4), i.e., the Brillouin function ( $B(J, a')$ ) [4]. Thus, one incorporates  $M_s(0)$ , which is obtained from DOS, and  $T_C$  into Eq. (4) to calculate  $M_s(T)$ :

$$\begin{aligned} M_s(T) &= M_s(0) \left( \frac{2J+1}{2J} \coth \left( \frac{2J+1}{2J} a' \right) - \frac{1}{2J} \coth \left( \frac{a'}{2J} \right) \right) \\ &= M_s(0) B(J, a'), \end{aligned} \quad (4)$$

where  $a' = \frac{M/M_0}{T/T_C} \left( \frac{3J}{J+1} \right)$  and  $J$  is the total angular momentum quantum number.

To calculate temperature-dependent magnetocrystalline anisotropy constant  $K(T)$ , we use the following Callen-Callen empirical relation (Eq. (5) [25]):

$$K(T) \propto K(0) [m(T)]^{n(n+1)/2} \quad (5)$$

where  $m(T)$  is the normalized saturation magnetization  $M_s(T)/M_s(0)$ , and  $n$  is the power of the anisotropy function. The  $n$  is 2 for uniaxial anisotropy.

## 4. Results and discussion

### 4.1. Magnetic moment

The total energy of TM (Fe, Co, or Ni)-doped  $L1_0$ -ordered MnAl was calculated using the equilibrium lattice parameters in Table 1 to determine the spin configurations. The volume and  $c/a$  ratio linearly decrease as valence electrons increase by substituting Mn with Fe, Co, and Ni in Table 1. The electron energy of the ferromagnetic arrangement between Mn and Fe or Co moments is lower than that of the antiferromagnetic structure of spins between them. On the other hand, when Ni substitutes

Mn, both spin and orbital moments of Ni are opposite to Mn's moment direction in Table 2, and the total energy of the opposite spin direction between Mn and Ni is lower than that of the same direction. Therefore, the total moment of Ni-doped MnAl is much lower than those of Fe- and Co-doped MnAl. These demonstrate that  $Mn_{0.5}Ni_{0.5}Al$  holds the ferrimagnetic spin configuration. In contrast, other substituted  $Mn_{0.5}TM_{0.5}Al$  (TM = Mn, Fe, or Co) are ferromagnetic because the spin and orbital moments of TM are aligned with the moments of Ni in the same direction.

Fig. 2 shows the density of states (DOS) for  $Mn_{0.5}TM_{0.5}Al$  (TM = Mn, Fe, Co, or Ni). The DOS significantly changes with TM substitution for Mn because the atomic valence electron configurations differ after substitution. When Fe or Co substitutes the Mn atom, the  $d$  band in the up-spin state insignificantly changes, but the down-spin pseudogap disappears for both Fe and Co-doped MnAl. The Fermi energy ( $E_F$ ) lies in the up-spin pseudogap for all  $Mn_{0.5}TM_{0.5}Al$  (TM = Fe, Co, and Ni). Valence electrons suppress (narrow) the pseudogap from Mn to Ni, suggesting that the stability of the compound decreases. Fe or Co substitution for Mn increases valence electrons of undoped-MnAl, which is a band-filling effect, resulting in enhanced spin polarization in the down-spin state. This leads to a lower magnetic moment. However, when Ni substitutes Mn, it appears that  $d-d$  hybridization becomes weak, and the down-spin pseudogap also disappears, suggesting unstable composition, i.e., antibonding appearance. Adding TM to  $L1_0$ -ordered MnAl enhances spin polarization in the down-spin state. The DOS analysis shows that  $Mn_{0.5}TM_{0.5}Al$  structures are less stable than  $L1_0$ -ordered MnAl. This is because the  $E_F$  of  $L1_0$ -ordered MnAl is located in the pseudogap in both up- and down-spin states, but the pseudogap in the down-spin state does not exist at the  $E_F$  for  $Mn_{0.5}TM_{0.5}Al$  (TM = Fe, Co, or Ni). In addition, the pseudogap of  $Mn_{0.5}TM_{0.5}Al$  (TM = Fe or Ni) is located below the  $E_F$ ; therefore, anti-bonding occurs between neighboring Fe or Ni and Mn atoms. To stabilize the doped  $L1_0$ -ordered MnAl, the  $E_F$  should be tuned to be located at the pseudogap by optimizing a doping element concentration.

Table 2 summarizes the calculated magnetic moments with corresponding saturation magnetization ( $M_s$ ) of  $Mn_{0.5}TM_{0.5}Al$ . The total magnetic moment per unit cell of TM-doped MnAl decreases with increasing valence electrons. It is noted that the spin and orbital moments of Ni become negative, suggesting the ferrimagnetic spin configuration of  $Mn_{0.5}Ni_{0.5}Al$ , as mentioned above. Fig. 3(a) shows the magnetic moment per unit cell of Fe-, Co-, or Ni-doped  $L1_0$ -ordered MnAl as a function of the number of valence electrons, i.e., substituting element. All calculated moments gradually decrease as the number of valence electrons increases. The calculated magnetic moment of  $L1_0$ -ordered, undoped MnAl is  $2.17 \mu_B / f.u.$ , which is smaller than  $2.40 \mu_B / f.u.$  in Ref. [2],  $2.37 \mu_B / f.u.$  in Ref. [3] and  $2.397 \mu_B / f.u.$  in Ref. [10]. Further, our calculated  $3.32 \mu_B / u.c.$  is also smaller than  $4.251 \mu_B / u.c.$  in Ref. [10] for  $Mn_{0.5}Fe_{0.5}Al$ . In electronic structure calculation, we used relaxed lattice parameters, but Sakuma and Manchanda used experimental room temperature lattice parameters. Manchanda et al. used the same lattice parameters as the lattice parameters of undoped MnAl for  $Mn_{0.5}Fe_{0.5}Al$ . Therefore, the differences between the moments in this study and the reported moments in Ref. [2,10] are attributed to using different lattice parameters in electronic structure calculations.

### 4.2. Magnetocrystalline anisotropy

We calculated the total energy difference between  $\langle 100 \rangle$  and  $\langle 001 \rangle$  spin configurations ( $\Delta E = E_{\langle 100 \rangle} - E_{\langle 001 \rangle}$ ) for magnetocrystalline anisotropy constant ( $K$ ). The calculated magnetocrystalline anisotropy energy (MAE) and constant ( $K$ ) are summarized in Table 3.

Fig. 3(b) shows the calculated  $K$  as a function of valence electrons, i.e., band filling. The  $K$  of undoped,  $L1_0$ -ordered MnAl is  $1.34 \text{ MJ/m}^3$ , and the easy axis is out-of-plane. When Fe substitutes for Mn, the  $K$  hugely increases to  $2.98 \text{ MJ/m}^3$  while retaining the out-of-plane magnetic anisotropy attributed to the change of valence electrons. This increasing

**Table 2**  
Calculated spin and orbital magnetic moments ( $\mu_B$ ) of  $L1_0$ -ordered  $Mn_{0.5}TM_{0.5}Al$ .

Material	Spin Moment ( $\mu_B$ )			Orbital Moment ( $\mu_B$ )			Total Moment ( $\mu_B/u.c.$ )	$M_s$ (emu/cm <sup>3</sup> )	$4\pi M_s/10000$ (T)
	Mn	TM	Al	Mn	TM	Al			
MnAl	2.16	2.16	-0.04	0.035	0.035	-0.0012	4.34	817.08	1.03
$Mn_{0.5}Fe_{0.5}Al$	1.99	1.30	-0.03	0.040	0.057	-0.0008	3.32	646.16	0.81
$Mn_{0.5}Co_{0.5}Al$	1.49	0.01	-0.02	0.020	0.004	-0.0005	1.49	301.58	0.38
$Mn_{0.5}Ni_{0.5}Al$	0.95	-0.06	-0.01	0.022	-0.005	-0.0004	0.89	179.16	0.23

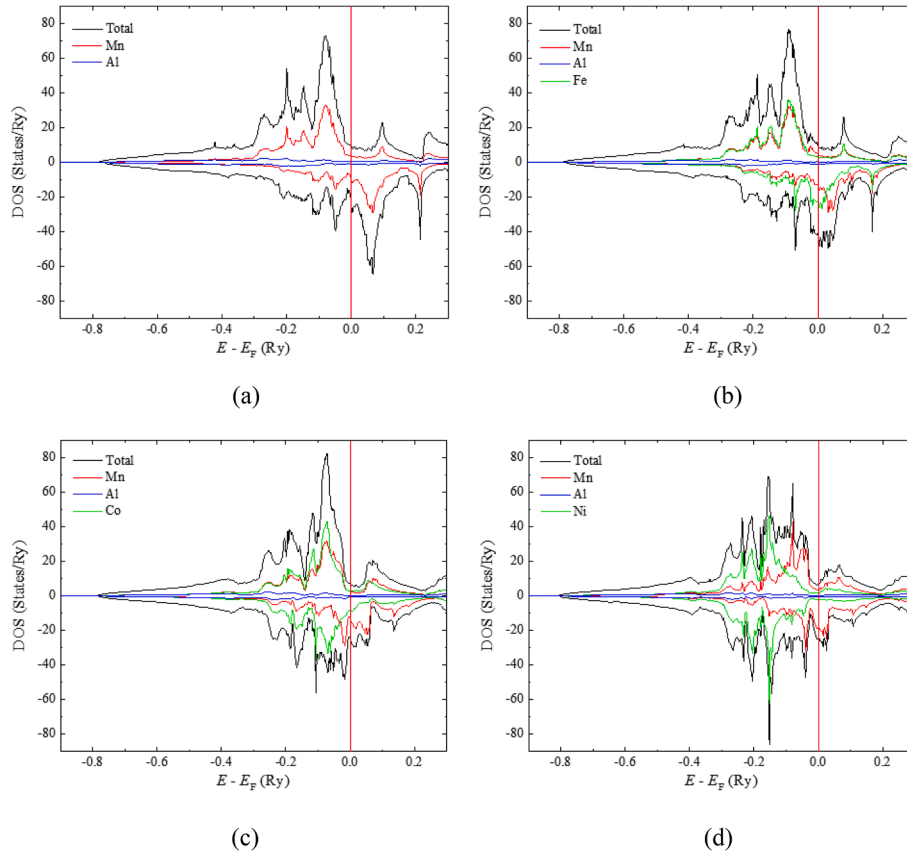


**Fig. 2.** Density of states (DOS) of (a)  $L1_0$ -ordered MnAl, (b)  $Mn_{0.5}Fe_{0.5}Al$ , (c)  $Mn_{0.5}Co_{0.5}Al$ , and (d)  $Mn_{0.5}Ni_{0.5}Al$ .

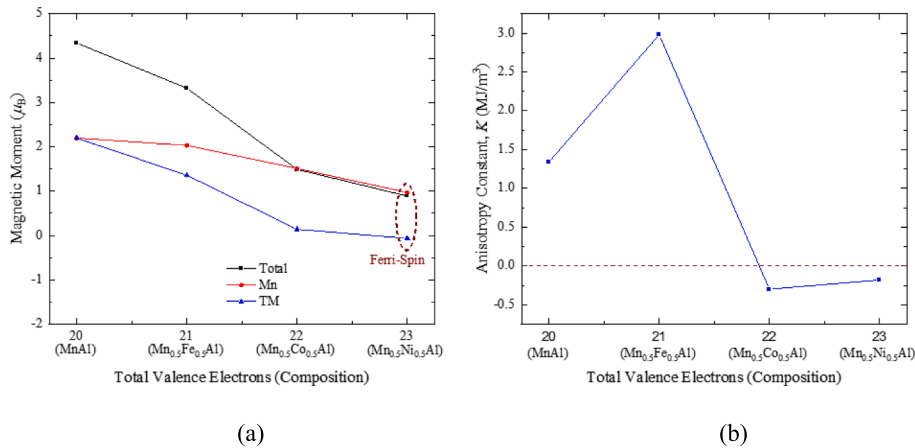


**Fig. 3.** (a) Calculated magnetic moments ( $\mu_B$ ) per unit cell and (b) calculated magnetocrystalline anisotropy constant of  $L1_0$ -ordered  $Mn_{0.5}TM_{0.5}Al$  (TM = Fe, Co, and Ni) at 0 K.  $n$  is the number of valence electrons for each substituting element.

**Table 3**

Magnetocrystalline anisotropy energy (MAE) and constant ( $K$ ) for  $L1_0$ -ordered  $Mn_{0.5}TM_{0.5}Al$  Alloys.

Material	MAE (meV/u.c.)	$K$ (MJ/m <sup>3</sup> )
MnAl	0.415	1.34
$Mn_{0.5}Fe_{0.5}Al$	0.885	2.98
$Mn_{0.5}Co_{0.5}Al$	-0.086	-0.30
$Mn_{0.5}Ni_{0.5}Al$	-0.051	-0.18

trend agrees with the result of Manchanda et al. [10]. However, our calculated  $K$  of 1.34 MJ/m<sup>3</sup> for  $L1_0$ -ordered MnAl is smaller than 1.50 MJ/m<sup>3</sup> in Ref. [2], 1.53 MJ/m<sup>3</sup> in Ref. [3], and 1.77 MJ/m<sup>3</sup> in Ref. [10]. This difference in  $K$  between this work and the reported ones is attributed to different lattice parameters used in calculating  $K$ . As mentioned in the previous section, Sakuma and Manchanda et al. used the lattice parameters measured at 300 K, while this work used fully relaxed (equilibrium) lattice parameters at 0 K in electronic structure calculations.

On the other hand, when Co or Ni substitutes Mn, the  $K$  becomes negative and changes from 1.34 MJ/m<sup>3</sup> to -0.3 MJ/m<sup>3</sup> for Co and -0.18 MJ/m<sup>3</sup> for Ni. Thus, the easy axis of Co- and Ni-substituted MnAl is in-plane, as shown in Fig. 4. The  $K$  increases as the number of valence electrons increases and reaches the maximum  $K$  at 8 of valence electrons and then decreases for a higher number of valence electrons than 8 in the Mn-TM-Al system [10,27,28]. This demonstrates that the magnetocrystalline anisotropy of  $L1_0$ -ordered MnAl can be tuned by partially substituting TM for Mn.

MAE is related to the bonding strength [26], explained by pseudo-gap in DOS. The bonding status for Fe-doped MnAl is antibonding because the pseudo-gap of spin-down DOS is located below Fermi energy. The MAE (or  $K$ ) can be explained by band filling [26]. The half occupation of the spin-down band (the number of valence electrons  $n = 7.5$ ) leads to the maximum MAE. The  $n$  for the 3d band is 7.5 (7 (Mn) + 8 (Fe) / 2) per formula unit of  $Mn_{0.5}Fe_{0.5}Al$ . Therefore, Fe-doping increases the MAE (or  $K$ ) mainly by band filling effect, as shown in Fig. 3 (b). The sign of MAE (or  $K$ ) changes to the negative when the  $n$  of the 3d band is higher than 7.5 but lower than  $n = 10.5$  in the spin-down band, including the 4s band. Co- and Ni-doped MnAl have  $n = 8$  (7 (Mn) + 9 (Co) / 2) and  $n = 8.5$  (7 (Mn) + 10 (Ni) / 2), respectively. These electron numbers are between 7.5 and 10.5. Therefore, our calculated  $K$  becomes negative, as shown in Fig. 3(b).

#### 4.3. Temperature dependence of saturation magnetization and magnetocrystalline anisotropy constant

To predict the temperature dependence of saturation magnetization

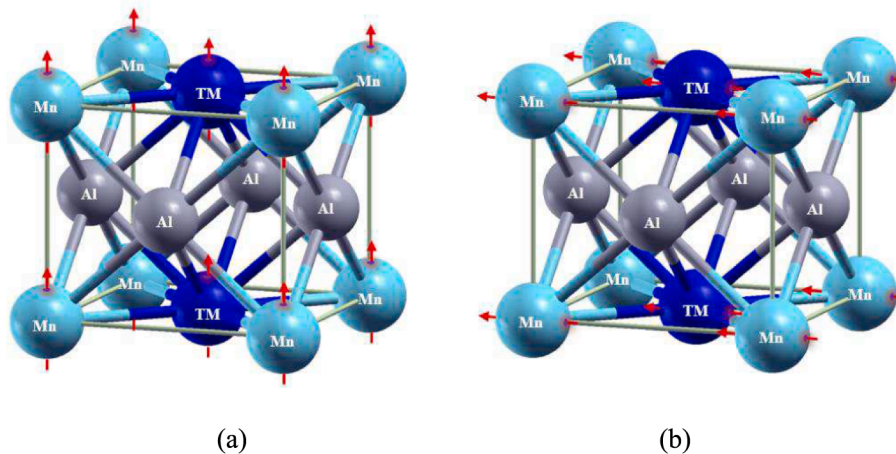


**Fig. 4.** (a) (001) (out-of-plane) and (b) (100) (in-plane) spin configurations of  $L1_0$ -ordered  $Mn_{0.5}TM_{0.5}Al$ .

$M_S(T)$  and magnetocrystalline anisotropy constant  $K(T)$ , one needs  $M_S(0)$  and exchange integral  $J_0$  to estimate Curie temperature ( $T_C$ ) of  $Mn_{0.5}TM_{0.5}Al$ . First, we calculated exchange integral  $J_0$  with the number of nearest neighboring atoms and the Curie temperature ( $T_C$ ) by using Eq. (3). Table 4 summarizes the geometric parameters used in calculating the  $T_C$ . The calculated  $T_C$  of  $L1_0$ -ordered, undoped MnAl is 685 K, close to 650 K in Ref. [7]. The  $T_C$  sharply decreases with Fe substitution but gradually decreases with Co and Ni substitutions. The exchange integral  $J_{ij}$  is related to the ratio of the interatomic distance between atoms [29–31]. Most contribution to  $J_0$  is from  $J_{02}$  ( $J_{Mn-Mn}$ ) between the nearest Mn atoms along the z-axis. The lattice constant  $c$  and  $J_0$  decrease as valence electrons increase from 7 (MnAl) to 11.5 ( $Mn_{0.5}Ni_{0.5}Al$ ), as Tables I and IV show. Therefore, the  $T_C$  decreases by substituting Mn with TM. MnAl shows the longest distance ( $r_{02}$ ) between Mn-Mn atoms along the c-axis and, consequently, the largest  $J_0$ . Ni-doping leads to the smallest  $J_0$ , therefore, the lowest  $T_C$  among the studied compositions. Our calculated  $M_S(0)$  and  $T_C$  reasonably agree with the results in Ref. [2,3,7,10].

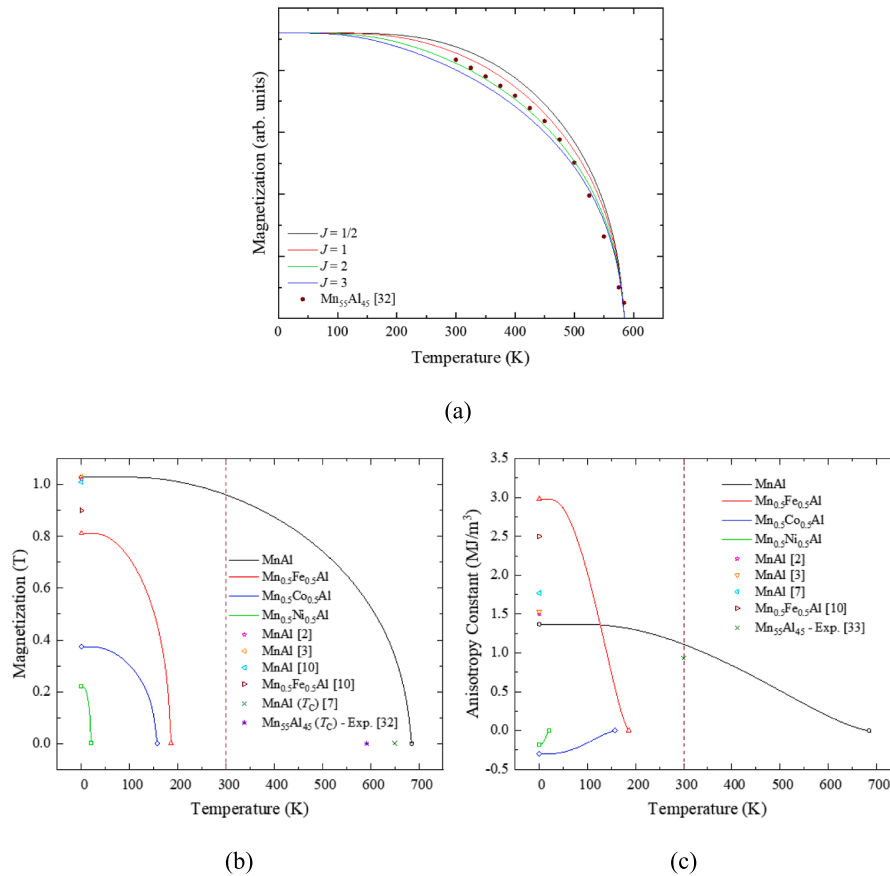
Now, the calculated  $M_S(0)$  in Table 2 and  $T_C$  in Table 4 are incorporated in the Brillouin function ( $B(J, a')$ ), i.e., Eq. (4), to investigate the thermal behaviors of saturation magnetization. To determine the total angular momentum quantum number ( $J$ ) in Eq. (4), we varied  $J$  between  $\frac{1}{2}$  and 3 and fitted Eq. (4) with experimental results in Ref. [32]. The  $M_S(T)$  with  $J = 2$  is well matched with the experimental results of  $Mn_{0.5}Al_{0.5}$  in Ref. [32], as shown in Fig. 5(a). Thus, we used  $J = 2$  to calculate  $M_S(T)$  for  $Mn_{0.5}TM_{0.5}Al$ .

Fig. 5(b) shows the  $M_S(T)$  for  $Mn_{0.5}TM_{0.5}Al$  (TM = Mn, Fe, Co, or Ni) estimated by Eq. (4). As the temperature increases, thermal disorder ( $kT$ ), i.e., thermal energy, increases against exchange energy ( $E_{ex}$ ) and opposes spontaneously aligned magnetic dipoles, forming spin cone. This implies that the width of the spin cone gets wider as temperature increases until the temperature reaches the paramagnetic state, resulting in the disappearance of magnetic ordering. It is noteworthy that the temperature dependence of saturation magnetization varies significantly among different compositions. This variation is associated with the magnetic anisotropy, as calculated in Fig. 5(c).

Regarding  $K(T)$ , the use of the semi-empirical Callen-Callen relation in Eq. (5) reveals thermal behaviors of magnetocrystalline anisotropy constant of  $Mn_{0.5}TM_{0.5}Al$  (TM = Mn, Fe, Co, or Ni) in Fig. 5(c).  $K(T)$  changes with  $M(T)/M(0)$  and by  $n(n+1)/2$  power law. Uniaxial crystal uses the  $n$  of 2 [4,25]. In this study, the MnAl structure is uniaxial; therefore, the  $n = 2$  was applied to the Callen-Callen relation in Eq. (5). Regardless of the out-of-plane or in-plane spin configuration, the magnetocrystalline anisotropy decreases as temperature increases for all the studied compositions. The  $K$  for the undoped-MnAl decreases slowly until 150 K but dramatically after 150 K in Fig. 5(c). The calculated 1.11

**Table 4**The number of the nearest neighbor ( $z_{0i}$ ), corresponding distance ( $r_{0i}$ ), sum of the exchange integrals ( $J_0$ ), and Curie temperature ( $T_C$ ) for  $L1_0$ - $Mn_{0.5}TM_{0.5}Al$ .

Material	The number of the nearest neighbor				Distance (Å)				$J_0$ (mRy)	$T_C$ (K)
	$z_{01}$	$z_{02}$	$z_{03}$	$z_{04}$	$r_{01}$	$r_{02}$	$r_{03}$	$r_{04}$		
MnAl	4	2	4	–	2.71	3.34	3.84	–	4.88	685
$Mn_{0.5}Fe_{0.5}Al$	4	2	2	4	2.72	3.21	3.21	3.85	1.32	186
$Mn_{0.5}Co_{0.5}Al$	4	2	2	4	2.84	2.87	2.87	4.01	1.12	157
$Mn_{0.5}Ni_{0.5}Al$	4	2	2	4	2.85	2.82	2.82	4.03	0.14	20

**Fig. 5.** (a) The temperature dependence of magnetization with various angular momentum quantum numbers ( $J = 1/2, 1, 2, 3$ ) for  $Mn_{55}Al_{45}$  and temperature dependence of (b) saturation magnetization ( $M_S$ ) with  $J = 2$ , and (c) magnetocrystalline anisotropy constant ( $K$ ) for  $Mn_{0.5}TM_{0.5}Al$ .

$MJ/m^3$  of  $K(300\text{ K})$  is close to the experimental  $K$  of  $0.93\text{ MJ/m}^3$  at  $300\text{ K}$  [33], but the  $K$  for TM-doped MnAl is negligible at  $300\text{ K}$  in Fig. 5(c). Co- and Ni-doped MnAl keep the in-plane magnetization, while the magnetization of Fe-doped MnAl is in the out-of-plane below its  $T_C$ . Magnetic ordering temperature, *i.e.*,  $T_C$ , is related to exchange integral ( $J_0$ ), which can be controlled by the doping element and its concentration. Therefore, the magnetic anisotropy of MnAl can be tuned by partially substituting TM for Mn.

## 5. Conclusion

The magnetocrystalline anisotropy of  $L1_0$ -ordered MnAl ( $\tau$ -phase) was tuned by partially substituting Mn of MnAl with the transition elements (Fe, Co, Ni). The Curie temperature sharply decreases with increasing the valence electrons by substituting Mn with Fe, Co, or Ni. The estimated magnetocrystalline anisotropy constant ( $K$ ) of  $Mn_{0.5}TM_{0.5}Al$  is  $1.34\text{ MJ/m}^3$  for  $TM = Mn$ ,  $2.98\text{ MJ/m}^3$  for  $TM = Fe$ ,  $-0.30\text{ MJ/m}^3$  for  $TM = Co$ , and  $-0.18\text{ MJ/m}^3$  for  $TM = Ni$ . Co- and Ni-substitutions change the magnetocrystalline anisotropy of MnAl to the in-plane direction. The  $K$  reaches a maximum of  $2.98\text{ MJ/m}^3$  at  $n = 8$ , *i.*

*e.*, Fe substitution.

## CRediT authorship contribution statement

**Minyeong Choi:** Methodology, Software, Validation, Formal analysis, Investigation, Writing – original draft, Writing – review & editing. **Yang-Ki Hong:** Conceptualization, Methodology, Software, Validation, Formal analysis, Investigation, Writing – original draft, Writing – review & editing, Supervision, Project administration, Funding acquisition. **Hoyun Won:** Formal analysis, Investigation, Writing – original draft. **Chang-Dong Yeo:** Conceptualization, Methodology, Software, Validation, Formal analysis, Investigation, Writing – original draft, Writing – review & editing, Supervision. **Nayem M.R. Shah:** Formal analysis, Investigation, Writing – original draft. **Byoung-Chul Choi:** Formal analysis, Investigation, Writing – original draft. **Woncheol Lee:** Formal analysis, Investigation, Writing – original draft. **Haein Choi-Yim:** Formal analysis, Investigation, Writing – original draft. **Wooyoung Lee:** Formal analysis, Investigation, Writing – original draft. **Jan-Ulrich Thiele:** Formal analysis, Investigation, Writing – original draft.

## Declaration of Competing Interest

The authors declare that they have no known competing financial interests or personal relationships that could have appeared to influence the work reported in this paper.

## Data availability

Data will be made available on request.

## Acknowledgment

This work was supported in part by the National Science Foundation IUCRC under Grant No. 2137275 and the E. A. “Larry” Drummond Endowment at the University of Alabama.

## References

- [1] D. Kramer, US government acts to reduce dependence on China of rare-earth magnets, *Phys. Today* 74 (2) (2021) 20, <https://doi.org/10.1063/PT.3.4675>.
- [2] A. Sakuma, Electronic Structure and Magnetocrystalline Anisotropy Energy of MnAl, *Journal of the Physical Society Japan* 63 (1994) 1422–1428, <https://doi.org/10.1143/JPSJ.63.1422>.
- [3] J.H. Park, Y.K. Hong, S. Bae, J.J. Lee, J. Jalli, G.S. Abo, N. Neveu, S.G. Kim, C. J. Choi, J.G. Lee, Saturation magnetization and crystalline anisotropy calculations for MnAl permanent magnet, *J. Appl. Phys.* 107 (2010) 09A731, <https://doi.org/10.1063/1.3337640>.
- [4] B.D. Cullity and C.D. Graham, *Introduction to Magnetic Materials*, 2nd ed., (Wiley, Hoboken, NJ, USA, 2009) p. 121, 139, 229, 374.
- [5] V. Seshu, T. Rajasekharan, Evidence of a critical Mn-Mn distance for the onset of ferromagnetism in NiAs type compounds, *J. Magn. Mater.* 42 (1984) 198–200, [https://doi.org/10.1016/0304-8853\(84\)90311-1](https://doi.org/10.1016/0304-8853(84)90311-1).
- [6] S. Sato, S. Irie, Y. Nagamine, T. Miyazaki, Y. Umeda, Antiferromagnetism in perfectly ordered L10-MnAl with stoichiometric composition and its mechanism, *Sci. Rep.* 10 (2020) 12489, <https://doi.org/10.1038/s41598-020-69538-2>.
- [7] J.M.D. Coey, Hard magnetic materials: a perspective, *IEEE Trans. Magn.* 47 (2011) 4671, <https://doi.org/10.1109/TMAG.2011.2166975>.
- [8] S. Kim, M. Choi, H. Won, H.-S. Lee, W. Lee, S.-G. Kim, W. Lee, Y.-K. Hong, Composition and property optimization of rare-earth-free Mn-Al-C magnet by phase stability and magnetic behavior analysis, *J. Alloy. Compd.* 919 (2022), 165773, <https://doi.org/10.1016/j.jallcom.2022.165773>.
- [9] X. Tong, P. Sharma, A. Makino, Investigations on low energy product of MnAl magnets through recoil curves, *J. Phys. D Appl. Phys.* 53 (2020), 175001, <https://doi.org/10.1088/1361-6463/ab7039>.
- [10] P. Manchanda, A. Kashyap, J.E. Shield, L.H. Lewis, R. Skomski, Magnetic properties of Fe-doped MnAl, *J. Magn. Mater.* 365 (2014) 88–92, <https://doi.org/10.1016/j.jmmm.2014.04.007>.
- [11] Z. Xiang, Y. Song, B. Deng, E. Cui, Y.u. Lunzhou, L.u. Wei, Enhanced formation and improved thermal stability of ferromagnetic  $\tau$  phase in nanocrystalline  $Mn_{55}Al_{45}$  alloys by Co addition, *Journal of Alloys Compounds* 783 (2019) 416–422, <https://doi.org/10.1016/j.jallcom.2018.12.350>.
- [12] Le Feng, Jens Freudenberger, Torsten Mix, Kornelius Nielsch, and Thomas George Woodcock, “Rare-earth-free MnAl-C-Ni permanent magnets produced by extrusion of powder milled from bulk,” *Acta Materialia* 199, 155–168 (2020). DOI: [doi.org/10.1016/j.actamat.2020.08.031](https://doi.org/10.1016/j.actamat.2020.08.031).
- [13] A. Morisako, N. Kohshiro, M. Matsumoto, Crystal structure and magnetic properties of Mn-Al-Ni films prepared by sputtering, *J. Appl. Phys.* 67 (1990) 5655, <https://doi.org/10.1063/1.346106>.
- [14] F. Jurries, J. Freudenberger, K. Nielsch, and Thomas George Woodcock, “The Influence of Cu-additions on the Microstructure, Mechanical and Magnetic Properties of MnAl-C Alloys”, *Sci. Rep.* 10 (2020) 7897, <https://doi.org/10.1038/s41598-020-64697-8>.
- [15] M. Sugihara, I. Tsuboya, *Structural and Magnetic Properties of Copper-Substituted Manganese-Aluminum Alloy*, *Jpn. J. Appl. Phys.* 2 (1963) 373–380.
- [16] H.X. Wang, P.Z. Si, W. Jiang, X.F. Xiao, J.G. Lee, C.J. Choi, M. Zhong, Z.F. Li, H. L. Ge, Structure and Magnetic Properties of Cu Doped MnAl, *Physical Science International Journal* 4 (4) (2014) 536–541, <https://doi.org/10.9734/PSIJ/2014/5326>.
- [17] L.e. Feng, J. Freudenberger, K. Nielsch, and Thomas George Woodcock, “Elimination of the non-recrystallised regions in the extruded MnAl-C-Ni magnet using pulverized melt-spun ribbons”, *J. Alloy. Compd.* 897 (2022), 163248 <https://doi.org/10.1016/j.jallcom.2021.163248>.
- [18] P. Blaha, K. Schwarz, F. Tran, R. Laskowski, G.K.H. Madsen, L.D. Marks, WIEN2k: An APW+lo program for calculating the properties of solids, *J. Chem. Phys.* 152 (2020), 074101, <https://doi.org/10.1063/1.5143061>.
- [19] A. Edstrom, J. Chico, A. Jakobsson, A. Bergman, J. Ruzs, Electronic structure and magnetic properties of  $L1_0$  binary alloys, *Phys. Rev. B* 90 (2014), 014402, <https://doi.org/10.1103/PhysRevB.90.014402>.
- [20] K. Schwarz, “Introduction to DFT and LAPW,” Satellite Meeting of the 32nd European Crystallographic Meeting (ECM32), Vienna, Austria (18. - 23. August 2019).
- [21] Mitchel Weissbluth, *Atoms and Molecules* (Academic Press, Elsevier Inc. 1978) p. 322–345. [22] P. Novák and J. Ruzs, “Exchange interactions in barium hexaferrite,” *Physical Review B* 71, 184433 (2005). DOI: [doi.org/10.1103/PhysRevB.71.184433](https://doi.org/10.1103/PhysRevB.71.184433).
- [22] I. Turek, J. Kudrnovský, V. Drchal, P. Bruno, Exchange interactions, spin waves, and transition temperatures in itinerant magnets, *Phil. Mag.* 86 (2006) 1713–1752, <https://doi.org/10.1080/14786430500504048>.
- [23] J.M. MacLaren, T.C. Schulthess, W.H. Butler, R. Sutton, M. McHenry, Electronic structure, exchange interactions, and curie temperature of FeCo, *J. Appl. Phys.* 85 (1999) 4833, <https://doi.org/10.1063/1.370036>.
- [24] H.B. Callen, E. Callen, The present status of the temperature dependence of magnetocrystalline anisotropy, and the power law, *J. Phys. Chem. Solid* 27 (1966) 1271–1285, [https://doi.org/10.1016/0022-3697\(66\)90012-6](https://doi.org/10.1016/0022-3697(66)90012-6).
- [25] D.-S. Wang, W.u. Ruqian, A.J. Freeman, *Phys. Rev. B* 47 (1993) 14932, <https://doi.org/10.1103/PhysRevB.47.14932>.
- [26] G. Meyer, J.-U. Thiele, Effective electron-density dependence of the magnetocrystalline anisotropy in highly chemically ordered pseudobinary (Fe1-xMnx)50Pt50 L10 alloys, *Phys. Rev. B* 73 (2006), 214438, <https://doi.org/10.1103/PhysRevB.73.214438>.
- [27] T. Suzuki, H. Kanazawa, A. Sakuma, Magnetic and structural properties of quaternary (Fe-Co-Ni)50Pt50 alloy thin films, *IEEE Trans. Magn.* 38 (2002) 2794, <https://doi.org/10.1109/TMAG.2002.803103>.
- [28] J.C. Slater, Cohesion in Monovalent Metals, *Phys. Rev.* 35 (1930) 509, <https://doi.org/10.1103/PhysRev.35.509>.
- [29] J.C. Slater, Atomic Shielding Constants, *Phys. Rev.* 36 (1930) 57, <https://doi.org/10.1103/PhysRev.36.57>.
- [30] A. Sommerfeld, H. Beter, 24, Part 2, in: H. Geiger, K. Scheel (Eds.), *Handbuch Der Physik*, Springer, Berlin, 1933, p. 595, [https://doi.org/10.1007/978-3-642-91116-3\\_3](https://doi.org/10.1007/978-3-642-91116-3_3).
- [31] A. Pasko, F. Mazaletat, M. LoBue, E. Fazakas, L.K. Varga, Hard magnetic properties of melt-spun Mn-Al-C alloys, *EPJ Web of Conferences* 40 (2013) 06008, <https://doi.org/10.1051/epjconf/20134006008>.
- [32] K. Kamino, T. Kawaguchi, M. Nagakura, Magnetic properties of MnAl system alloys, *IEEE Trans. Magn.* 2 (1966) 506–510, <https://doi.org/10.1109/TMAG.1966.1065887>.